compression ratios in excess of 1.5 correspond to $\lambda > 1$ and should result in materials with negative Poisson's ratio determined by formulae (1) and (2).

To check theoretical conclusions, we carried out a computer simulation of two plane networks. The first network consisted of straight elastic bar elements, the second consisted of compressed elements with a kink angle corresponding to a compression ratio of ~1.6 ($\lambda = 2$). The original and the compressed network are shown in Fig. 3*a* and *b*. Both networks were compressed uniaxially. Figure 3*c* and *d* illustrate the results of these simulations by showing trajectories of network nodes under uniaxial compression. The original network has $\nu = 0.33$, whereas the compressed network has $\nu = -0.25$, as determined by equation (2).

The generality of the theory can be tested by applying it to a class of molecular systems. Wojciechowski[9] suggests that solids consisting of nonconvex hexagon-type molecules (hexamers) may have negative Poisson's ratio. Such molecules can be modelled in two dimensions by rigidly connected discs ('atoms') at the vertices of a hexagon (Fig. 4*a*). If discs are assumed to be soft at the exterior and have a hard elastic core, neighbouring molecules can interpenetrate (Fig. 4*b*). Wojciechowski[9] has shown, both theoretically and using numerical simulations, that such a system has negative Poisson's ratio when interpenetration of particles is large. As hexamer particles are roughly circular, their interactions are not far different from interactions between sand particles. Although the contact cannot be treated as a point, there is still a force acting between particles, with a component f_n along a line connecting particle centres as well as a component f_t acting perpendicular to this line (Fig. 4*c*). Both force components cause displacements in their respective directions, as in the case of sand particles. If the core of hexamer 'atoms' is assumed elastic, normal and tangential force components will be proportional to the corresponding displacements, and the parameter $\lambda = k_t/k_n$ can be calculated. Figure 4*c* illustrates the dependence of λ on the interpenetration of molecules, expressed in terms of a ratio of the original cell dimension to the reduced cell size. Different cell geometries are modelled by changing the diameter of the elastic core while preserving the distance between vertices of the perimeter molecules.

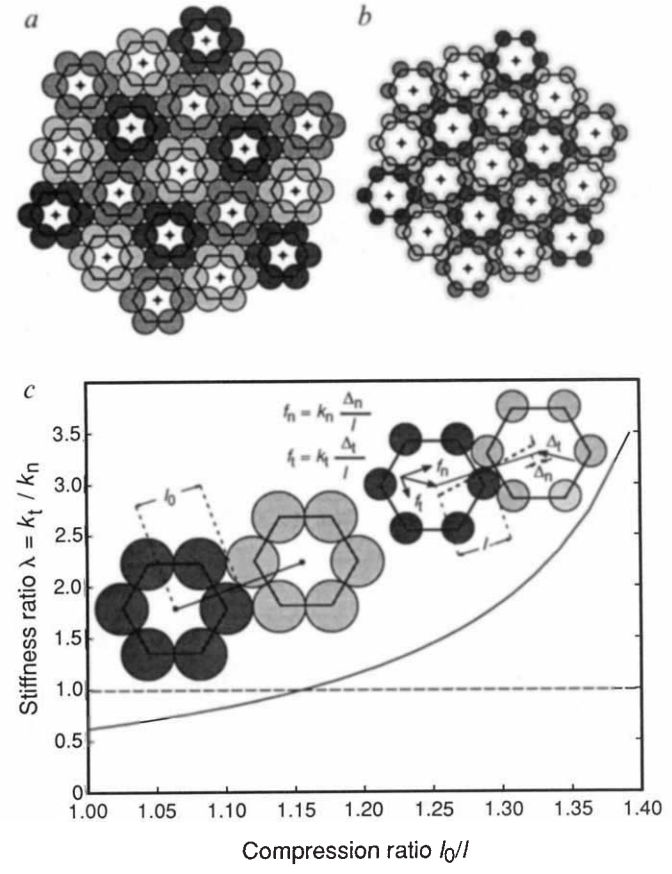

FIG. 4 *a*, Two-dimensional hexagonal array of rigidly connected discs. *b*, Interpenetration of these discs, assumed to be soft at the outside and to have a hard elastic core. Individual 'molecules' are indicated by the shading. *c*, Stiffness ratio as a function of compression ratio for the array of discs. Poisson's ratio becomes negative when $\lambda > 1$, which occurs at high interpenetration.

Interpenetration of the hexamer particles reduces the normal stiffness whereas the tangential stiffness increases. When the diameter of the elastic core is 0.7 of the particle diameter, both stiffness components become equal ($\lambda = 1$) and $\nu = 0$. For larger interpenetrations, Poisson's ratio becomes negative. Wojceichowski[9], using a completely different analysis, reaches virtually identical conclusions.

Strictly, the analysed hexamer system is an anisotropic crystal with a 6-fold symmetry. Similar systems are known to behave as isotropic solids as far as deformation properties are concerned. It is not difficult to construct a truly isotropic system with the same type of behaviour. Any assembly of particles with nonconvex surfaces that allow sufficient interpenetration should show a negative Poisson's ratio. The main cause of this unusual behaviour is greater stiffness of microstructural elements in shear than in compression. □

Received 30 August; accepted 3 October 1991.

1. Love, A. E. H. *Mathematical Theory of Elasticity* (Dover, New York, 1944).
2. Caddock, B. D. & Evans, K. E. *J. Phys. D: Appl. Phys.* **22,** 1877–1882 (1989).
3. Evans, K. E. *J. Phys. D: Appl. Phys.* **22,** 1870–1876 (1989).
4. Lakes, R. *Science* **235,** 1038–1040 (1987).
5. Bathurst, R. J. & Rothenburg, L. *Int. J. Engng Sci.* **26**(4), 373–383 (1988).
6. Mindlin, R. D. *J. appl. Mech.* **16,** 259–268 (1949).
7. Almgren, R. F. *J. Elasticity* **15,** 427–430 (1985).
8. Green, L. J. & Ashby, M. F. *Cellular Solids* (Pergamon, Oxford, 1988).
9. Wojciechowski, K. W. *Phys. Lett.* A**137,** 60–64 (1989).

Organic matter and containment of uranium and fissiogenic isotopes at the Oklo natural reactors

Bartholomew Nagy*, F. Gauthier-Lafaye†, P. Holliger‡, D. W. Davis§, David J. Mossman‖, Joel S. Leventhal¶, Mark J. Rigali* & John Parnell#

* Laboratory of Organic Geochemistry, Department of Geosciences, The University of Arizona, Tucson, Arizona 85721, USA
† Centre National de la Recherche Scientifique, Centre de Géochimie de la Surface, 1 Rue Blessig, 67084 Strasbourg Cedex, France
‡ Centre d'Etudes Nucléaires de Grenoble, 38041 Grenoble Cedex, France
§ Geology Department, Royal Ontario Museum, 100 Queen's Park, Toronto, Ontario M5S 2C6, Canada
‖ Department of Geology, Mount Allison University, Sackville, New Brunswick E0A 3C0, Canada
¶ US Geological Survey, Federal Center, MS 973, Denver, Colorado 80225, USA
# Department of Geology, The Queen's University of Belfast, Belfast BT7 1NN, Northern Ireland

SOME of the Precambrian natural fission reactors at Oklo in Gabon contain abundant organic matter[1,2], part of which was liquefied at the time of criticality and subsequently converted to a graphitic solid[3,4]. The liquid organic matter helps to reduce U(VI) to U(IV) from aqueous solutions, resulting in the precipitation of uraninite[5]. It is known that in the prevailing reactor environments, precipitated uraninite grains incorporated fission products. We report here observations which show that these

© 1991 Nature Publishing Group

uraninite crystals were held immobile within the re-solidified, graphitic bitumen. Unlike water-soluble (humic) organic matter, the graphitic bituminous organics at Oklo thus enhanced radionuclide containment. Uraninite encased in solid graphitic matter in the organic-rich reactor zones lost virtually no fissiogenic lanthanide isotopes. The first major episode of uranium and lead migration was caused by the intrusion of a swarm of adjacent dolerite dykes about 1,100 Myr after the reactors went critical. Our results from Oklo imply that the use of organic, hydrophobic solids such as graphitic bitumen as a means of immobilizing radionuclides in pretreated nuclear waste warrants further investigation.

Small pockets of uranium ore at Oklo went critical 1,950 ± 30 Myr ago[6], producing several natural fission reactors. Reactors 1–6 contain virtually no organic matter. Total energy production in these reactors was 16,500 MW yr. Roughly 6 tons of ^{235}U fissioned; the total uranium content was 800 tons. Reactors 7–9 contain abundant organic matter with heterogenous distributions. They produced 1,300 MW yr of energy, and 480 kg of ^{235}U fissioned; their total uranium content[6] was 80 tons. The reactors are located in the C-1 stratum of the Proterozoic Francevillian Series, which consists of sedimentary rocks[7,8]. Nuclear fission reactions occurred in ores with 25–60% uranium. Water acted as a moderator; the reactions ceased after 10^5–10^6 years (ref. 9) when too little fissile material remained. Temperatures during criticality ranged between 160 and 360 °C in the reactors[7,9]. Organic matter in reactors 7–9 consists of kerogen and now solid bitumen[4,10,11].

Organic matter in the Oklo natural reactors 7–9 could have important effects on radionuclide containment. This assumption is based on observations at other uranium deposits[12], where solid organic matter prevented the movement of uraninite, uranium and radiogenic products. Although liquid bitumen was generated by hydrothermal solutions from the uraniferous organic solid in these deposits[12], migration and leaching of uraninite and radionuclide mobilization by bitumen were minimal. Our aim was therefore to determine whether the same occurred at Oklo and, if it did, whether one could thereby learn lessons for nuclear waste storage.

The following sequence of events is known to have occurred in radionuclide containment at Oklo. First, liquid bitumen was derived from syngenetic kerogen through hydrothermal processes[13] at the time of criticality[14]. Second, the abundant liquid bitumen (and less-available kerogen) reduced U(VI) from aqueous solutions (possibly by π-electron, redox atom transfer and/or radiation-induced reduction, each involving organics). This resulted in the precipitation of uraninite, in which fission products were incorporated. Next, liquid bitumen was intruded into fractures and pores[3] during and after criticality. Finally, bitumen solidified at these sites, immobilizing the enclosed uraninite. Heat soon turns bitumen into a solid containing cryptocrystalline graphite[15].

Migration of liquid bitumen in the reactors and surrounding rocks is revealed by organic petrography, which shows narrow (micrometre-sized) and wider (millimetre or centimetre-sized) fractures, intruded by and filled with bitumen[2], as well as granular bitumen filling the pore and void spaces in rocks (Table 1, column 3). The non-mobilized organic matter is kerogen, which is a syngenetic solid[14]. Electron microprobe analyses showed that kerogen and bitumen in and near the reactors (at least 200 m away) contains mainly micrometre-sized dispersed uraninite. Bitumen also contains crystals of galena which represent, in part, precipitated radiogenic lead. Distant organic samples contain no uraniferous minerals. Reflected light microscopy showed textural features indicating that uraninite was not effectively mobilized by bitumen, which became increasingly viscous and then solidified before much migration and transport of uraninite could occur. Solidification and graphitization of bitumen were caused by the heat in the reactors (the temperature varied in space and time).

TABLE 1 Constituents of organic-rich sedimentary rocks in and near Oklo natural fission reactors

Sample number	Sample location	Organic constituents	Kerogen $R_{o,max}$(%), $R_{o,min}$(%) $\bar{R}_{o,max}$(%)
1	Reactor 7 within reactor core	Kerogen particles; granular bitumen	3.58, 0.98 2.57 (n=47)
2	Reactor 9 at reactor core edge	Kerogen particles; bitumen in veins	3.52, 1.23 2.22 (n=41)
3	At reactor core edge	Galena crystal, isolated from organic matter	ND, inorganic phase
4	At reactor core edge	Kerogen in two populations; abundant bitumen	3.24, 1.24 2.49 (n=38)
5, 6	1.2 m from reactor core	Granular bitumen; kerogen particles	ND
7	Reactor 8, 50 m from reactor core	ND	ND
8, 9, 10	Reactor 9, 200 m from reactor core	Bitumen in veins; kerogen particles	4.54, 0.77 3.08 (n=36)
11	5 km from the reactors at the Boyindzi U ore deposit	Bitumen in veins; kerogen particles	6.04, 0.89 3.93 (n=37)
12	8 km from the reactors, from a vein traversed by drill core	Highly solidified, vitreous organic matter derived from bitumen	5.16, 3.78 4.95 (n=25)
13	50 km from the reactors, FB black shale	Abundant kerogen, 'coked' equivalent of bitumen	5.18, 4.02 5.01 (n=5)

ND, not determined. Reflectance measurements, in oil, were made on kerogen using a Zeiss Axioskop microscope under incident white and blue light, and a six-in-one standard (R_o=0.3–1.68%). $R_{o,max}$, $R_{o,min}$ are maximum and minimum reflectances, measured in oil. $\bar{R}_{o,max}$ is the mean maximum reflectance for n measured points. Gas chromatography mass spectrometry (discussed in the text) was carried out at 450 °C and 900 °C, with a Chemical Data Systems Pyroprobe coupled to a Hewlett-Packard 5710A gas chromatograph (25 m × 0.31 mm internal diameter, 5% phenyl methyl silicone, fused silica column) and a Finnegan MAT model 700 mass spectrometer with ion trap detector. Mineral constituents were identified with a JEOL-733 electron microprobe. Microfocused laser Raman spectra (discussed in the text) were obtained with a 25-W Ar laser, using 544-nm light, with 60–90 mW, transmitted to an Olympus BH2 microscope and to a Jobin Yvon model U spectrometer.

Migration of uraninite in bitumen has also been very limited at the 2,300-Myr-old Elliot Lake uranium deposits in Canada[12]. In bitumen, uraninite microcrystals were virtually unleached, and uranium, thorium, samarium and so on were insoluble and did not migrate[12], just like at Oklo. But humic materials, which contain carboxyl and similar groups, readily form complexes with uranium and other actinide elements, and form colloids affecting radionuclide migration in groundwater[16]. Humic colloids can remain in suspension in water for a long time and are known to be transported over significant distances by groundwater[17]. Such radionuclide migration did not occur at Oklo. Solid bitumen in the Oklo reactors contained highy condensed aromatic hydrocarbons with abundant, dispersed cryptocrystalline graphite, but no detectable carboxyl groups[3]. Therefore, this solid Oklo organic substance did not form colloids, could not migrate and was not a vehicle for actinide transport. Thus, organic solids consisting of highly condensed aromatic hydrocarbons and abundant graphite effectively contain uraninite and radionuclides.

Bitumen and kerogen in and near the reactors have less graphitic and less tightly bound structures than distant organics. Uraninite and fissiogenic isotopes may be more easily released from these structures, enhancing radionuclide loss from the reactors; this possibility had to be tested. Microfocused-laser Raman spectra showed that the hydrocarbons in and around the reactors contain cryptocrystalline graphite of smaller particle sizes than organic matter at the distant (8, 50 km) locations. In and near the reactor cores, reflectances of organic matter are relatively low. At sites distant from the reactors, reflectances are high because graphitization is better developed and molecular condensation of aromatic hydrocarbons is more extensive (Table 1, column 4). Pyrolysis/gas-chromatography/mass spectrometry

© 1991 Nature Publishing Group

TABLE 2 Isotope ratios and $^{207}Pb/^{206}Pb$ ages of samples in and near the organic-rich Oklo natural fission reactors

Isotope ratios of U and Pb and Pb–Pb ages of organic matter containing minute dispersed minerals.

Sample number	$^{235}U/^{238}U$	U (p.p.m.)	Pb (p.p.m.)	$^{204}Pb/^{206}Pb$*	$^{207}Pb/^{206}Pb$*	$^{208}Pb/^{206}Pb$*	$^{206}Pb/^{238}U$†	$^{207}Pb/^{235}U$†	$^{207}Pb/^{206}Pb$† Age (Myr)
2‡	0.00725	103,000	13,150	0.000128	0.09684	0.00633	0.13458	1.7659	1,529
3‡	ND	30	558,000	0.000153	0.11138	0.00783	ND	ND	1,788
4‡	0.00716	4,150	7,910	0.000212	0.12453	0.01090	1.9451	32.994	2,004
5‡	ND	<10	102	0.000730	0.04579	0.03160	ND	ND	−707
6‡	ND	14	215	0.000417	0.06464	0.02433	ND	ND	554
7‡	0.00725§	11,930	9,200	0.000169	0.11477	0.00858	0.7975	12.437	1,851
8§	0.00725	ND	ND	0.000024	0.06360	0.00084	0.0763	0.665	717
	0.00725	ND	ND	0.000021	0.06314	0.00076	0.0665	0.576	704
	0.00725	ND	ND	0.000012	0.06182	0.00048	0.0720	0.612	665
	0.00725	ND	ND	0.000019	0.06214	0.00064	0.0512	0.437	670
	0.00725	ND	ND	0.000024	0.06384	0.00093	0.0814	0.713	730
	0.00725	ND	ND	0.000025	0.06377	0.00091	0.0626	0.547	722
	0.00725	ND	ND	0.000015	0.06271	0.00078	0.0724	0.624	690
	0.00725	ND	ND	0.000015	0.06226	0.00059	0.0774	0.662	675
9§	0.00725	ND	ND	0.000015	0.06300	0.00068	0.1026	0.887	700
	0.00725	ND	ND	0.000020	0.06270	0.00059	0.1002	0.860	683
	0.00725	ND	ND	0.000018	0.06350	0.00066	0.1006	0.876	715
	0.00725	ND	ND	0.000014	0.06443	0.00058	0.1091	0.964	745
	0.00725	ND	ND	0.000025	0.06450	0.00099	0.1026	0.906	742

Isotope ratios of U, Mo, Ag, Sn, Te, Nd and Sm

Sample number	$^{235}U/^{238}U$	Mo‖ 98/95	Ag‖ 109/107	Sn‖ 120/124	Te‖ 128/130	Nd§ 144/143	Sm§ 149/147
Natural isotopic ratios	0.00725	1.5	0.92	5.7	0.90	1.95	0.92
1	0.00678¶	—	0.49#	—	0.18#	1.14¶	0.03¶
2	0.00725‡	1.5	—	6.0	0.40	1.27	0.45
4	0.00716‡	1.1	0.60	5.0	0.17	—	0.12
5	—	1.4	—	6.0	—	—	0.90¶
7	0.00725§	1.5	0.60	5.2	0.14	1.84	0.78
Fission product ratios	—	0.90	0.30	0.5	0.18	1.11	<0.1

Decay constant $\lambda_{^{238}U}=0.15513\times10^{-9}\,yr^{-1}$, $\lambda_{^{235}U}=0.98485\times10^{-9}\,yr^{-1}$; normal $^{235}U/^{238}U=0.00725$. ND, not determined. Fission product ratios (bottom of table) are theoretical and adjusted for published parent abundances[18] in reactor 9.

* Corrected for fractionation and blank only.

† Corrected for fractionation, blank and common lead; age data were calculated using measured U isotopic compositions; 2σ errors are 2–4 Myr.

‡ Lead and uranium isotopes measured with a VG354 thermal ionization mass spectrometer following dissolution of samples in a mixture of $HClO_4$, HNO_3 and HF, spiking of aliquots with ^{205}Pb and ^{235}U and standard column separation procedures (except where noted otherwise); samples were individual grains weighing 10–50 μg. 2σ error range is ±0.1–0.2% for all $^{207}Pb/^{206}Pb$ and $^{238}U/^{235}U$ ratios.

§ Determined with CAMECA IMS3f ion microprobe mass spectrometer on individual uraninite crystals[23]; typical spot analysed was 20 μm in diameter. 2σ error range is 0.1%, 0.5% and 1.0% for $^{207}Pb/^{206}Pb$, $^{206}Pb/^{238}U$ and $^{207}Pb/^{235}U$ ratios, respectively, with a precision of 0.08% after correction for mass discrimination effect (0.2% per a.m.u.). Accuracies of U, Nd, and Sm isotope ratios are ±0.02, ±0.02 and ±0.01, respectively.

‖ Measured with VG PQII inductively coupled plasma mass spectrometer in argon, after laser ablation of polished surfaces using a Spectron neodymium–yttrium–aluminium garnet laser to volatilize millimetre-sized areas of organic samples. Accuracy of the isotope ratios measured by this mass spectrometer is ±0.1 for Mo and Ag, and ±1 for Sn and Te.

¶ Analyses done on 10-mg powdered sample by thermal ionization mass spectrometry. Results permit calculation of the apparent age of fission reaction: $age=1/\lambda_5\ \ln(AN_f/U\tau)$, where λ_5 is the radioactive decay constant of ^{235}U, N_f/U is the number of fissions of ^{235}U relative to present-day U; the abundance of fissiogenic Nd is directly related to the ^{235}U content involved in the fission reactions and is used to define the value of N_f. τ is the fluence received by the sample, and A is a factor of nuclear parameters of samples and spectrum index[26]. The mean Nd age of three samples at reactor core 9 is 1,300 Myr; the age of sample 1 within reactor 7 is 1,850 ± 15 Myr.

Calculated from ref. 28.

confirmed this trend. The thermal energy imparted by the pyrolysis experiment was less capable of fragmenting bitumen and kerogen structures in distant samples than the less tightly bound organic solids in and around the reactors. Hydrothermal reactions and radiation, leading to addition of H , H_2 and so forth, and neutron fluence are the most likely explanation for the less tightly bound organic structures at the reactors. Uraninite crystals remained immobile within this solid organic matter. Microscopic observations revealed no evidence that hydrothermal effects and radiation damage dislodged uraninite from the graphitic bitumen and kerogen in and around the reactors.

Ion microprobe mass spectrometry showed that several fission products were incorporated in this uraninite when it precipitated at the edge of the reactor cores (Table 2). Molybdenum and tin show no abnormal isotopic compositions, whereas silver, tellurium, neodymium and samarium have large fissiogenic contributions even at a distance of 50 m from the reactor core (Table 2, sample 7). This is in agreement with previous findings[18] in the peripheral rocks of reactor 9. Migration of fission products to limited distances from the reactor core was possibly caused during criticality by convective aqueous solutions, before hot water could generate enough bitumen to precipitate uraninite, which incorporates fission products. Reactor 9 contains uraninite both enclosed in organic matter (from which nuclides were not lost) and enclosed in clays (from which neodymium was lost). As much as 30% of fissiogenic neodymium, relative to uranium, has been lost by those samples[19,20] that are most depleted in ^{235}U, in reactor core 9. Similarly, restricted local migration of lanthanides was observed[21] from uraninite not protected by organic matter in reactor core 2, which contains clays but virtually no organics. In contrast, sample 1 in reactor core 7, where uraninite is enclosed in organic matter, shows near-normal fission product ratios and insignificant migration of fissiogenic isotopes, especially neodymium (Table 2). On the basis of these measurements, clay minerals seem to be less effective than organic matter at preventing the release of uranium and fissiogenic isotopes.

Isotopic analyses by thermal ionization mass spectrometry

© 1991 Nature Publishing Group

indicate varying uranium and lead mobilities. Uranium from bitumen in a vein at the edge of reactor core 9 shows no $^{235}U/^{238}U$ depletion, whereas that from an unfractured sample shows $^{235}U/^{238}U$ depletion, indicating influx of isotopically normal uranium through fractures after the reactor went critical. The isotopes ^{238}U and ^{235}U naturally decay to radiogenic, non-fissiogenic ^{206}Pb and ^{207}Pb, respectively, allowing determination of radiometric ages, which should be the same for coeval samples that were part of closed systems. Organic-rich samples 2, and 4–7 give dissimilar $^{207}Pb/^{206}Pb$ ages (Table 2), indicating that the samples had been open systems with respect to uranium and lead migration. Migration of mobile intermediate decay products such as ^{222}Rn and/or ^{226}Ra (refs 22, 23) into samples 5 and 6, which have very low lead and uranium concentrations, would lead to excess ^{206}Pb and might explain their low (and negative) $^{207}Pb/^{206}Pb$ ages. Galena (sample 3) contains radiogenic lead with a $^{207}Pb/^{206}Pb$ age of 1,788 ± 4 Myr, indicating that this lead evolved in a uraniferous closed system until the late Phanerozoic. The three organic samples that contain sufficient uranium to plot on a concordia diagram (Fig. 1*a*) show considerable lead and/or uranium mobility. Data points from closed systems would lie on the concordia curve. Points above concordia are from samples that have lost uranium and/or gained radiogenic lead, points below are for samples that have gained uranium and/or lost radiogenic lead. Data from minerals suffering only one episode of lead–uranium mobility should lie along a line whose upper and lower concordia intersections give the ages of primary formation and mobilization, respectively. The scatter of data points around the best-fit line in Fig. 1*a* is outside analytical error, indicating that mobilization of lead and uranium occurred more than once. The lower concordia intersection of 330 Myr should represent an approximate average age of mobility. Although the points reveal substantial disturbance (50–80%), their scatter could be accounted for by a minimum of 300 Myr (330 ± 150 Myr) duration of mobility, suggesting containment long after criticality. The cause of this mobilization is unknown, because rocks of this age are absent in Gabon.

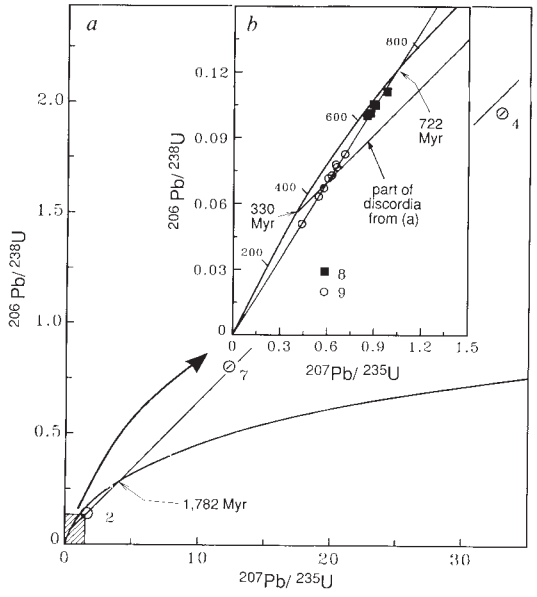

FIG. 1 *a*, Concordia plot showing U/Pb isotope analyses by thermal ionization mass spectrometry of three uraniferous organic samples from Oklo. The line is the calculated best-fit regression to the three points. The U/Pb ratios are very disturbed and the scatter in the points is well outside analytical error. Numbers 2, 4, 7, 8 and 9 refer to sample numbers in Tables 1 and 2. *b*, Concordia plot showing U/Pb isotope analyses by ion microprobe mass spectrometry of thirteen uraninite grains in organic matter in samples 8 and 9, located 200 m from reactor 9 and 50 m from a dolerite dyke intrusion. The best-fit line for discordia was calculated following the procedure of Ludwig[27]. The error is given at 2σ (95% confidence level). Uranium and lead mobilization age (T_2) is 722 ± 30 Myr. T_1 = 1,850 ± 15 Myr defines the apparent time at which natural reactors 7–9 went critical. It was calculated as follows: $(^{207}Pb/^{206}Pb)_{radiogenic}$ = present $(^{235}U/^{238}U) \times 10^{-2} \times [\exp(\lambda^{235}_{U} T_1) - \exp(\lambda^{235}_{U} T_2)]/[\exp(\lambda^{238}_{U} T_1) - \exp(\lambda^{238}_{U} T_2)]$, where $(^{207}Pb/^{206}Pb)_{radiogenic}$ is the radiogenic lead in galena. T_1 was calculated on the basis of $^{207}Pb/^{206}Pb = 0.1405 \pm 0.0015$ (2σ), which is the mean value of seven individual galena crystals analysed from reactors 7–9.

Individual uraninite grains were analysed by ion microprobe mass spectrometry. This method ensures that different mobilities of uranium and lead are recognized in uraninite crystals of different environmental histories. These grains were enclosed in graphitic organic matter in two samples located 200 m from reactor 9 and only 50 m from a major intrusive dolerite dyke of the dyke-swarm, which was dated[24] at 750 ± 150 Myr. An upper concordia intersection of 722 ± 30 Myr (Fig. 1*b*) was obtained[25]. Data points show low scatter along the discordia. An episode of uranium and lead mobilization, and uraninite and galena crystallization, therefore occurred at 722 ± 30 Myr age and was caused by the intrusion of an adjacent ~15-m-wide dolerite dyke and the extensive dyke-swarm. Apparently the first large migration of U and Pb (and various fissiogenic isotopes) occurred at ~1,100 Myr after the reactors went critical at Oklo, because of the onset of a major, adjacent tectonic–igneous event. Some earlier migration, possibly caused by minor tectonic events, cannot be ruled out, but the limited scatter of data points 2, 7 and 4 (Fig. 1*a*) suggests that this was probably minor.

We conclude that immobilization of uraninite in solid graphitic organic matter enhanced the containment of ^{235}U and a number of fissiogenic isotopes at the Oklo natural reactors. Therefore, we suggest that the same containment mechanism should be considered for the burial of anthropogenic nuclear waste products. It should be noted, however, that the very specific processes leading to immobilization at Oklo are not simply analogous to the enclosure of a radionuclide-containing inorganic solid in highly graphite bitumen. Nevertheless, other characteristics of solid bitumen, such as its hydrophobicity, inducible plasticity and nonflammability, should encourage us to explore this avenue for waste containment. □

Received 10 April; accepted 5 November 1991.

1. Geoffroy, J. *The Oklo Phenomenon*, 133–149 (IAEA, Vienna, 1975).
2. Alpern, B. *Natural Fission Reactors*, 333–351 (IAEA, Vienna, 1978).
3. Leventhal, J. S., Nagy, B. & Gauthier-Lafaye, F. *US Geol. Surv. Open-File Rep.* 89-668, 1–18 (1989).
4. Cortial, F., Gauthier-Lafaye, F., Lacrampe-Couloume, G., Oberlin, A. & Weber, F. *Org. Geochem.* **15,** 73–85 (1990).
5. Choppin, G. R. & Rydberg, J. *Nuclear Chemistry: Theory and Applications*, 235 (Pergamon, Oxford, 1980).
6. Naudet, R. *Oklo: des Réacteurs Nucléaires Fossiles*, 695 (ed. le Commisariat à l'Energie Atomique, Paris, 1991).
7. Gauthier-Lafaye, F., Weber, F. & Ohmoto, H. *Econ. Geol.* **84,** 2286–2295 (1989).
8. Gauthier-Lafaye, F. & Weber, F. *Econ. Geol.* **84,** 2267–2285 (1989).
9. Holliger, P. & Devillers, C. *Earth planet. Sci. Lett.* **52,** 76–84 (1981).
10. Bros, R., Gauthier-Lafaye, F., Stille, P. & Clauer, N. *Symp. Metalliferous Black Shales and Related Ore Deposits, IGCP Proj. 254*, Abstr. 1 (1990).
11. Bostick, N. H., *Aspects of Diagenesis, Soc. Econ. Palaeont. Mineral. Spec. Publ.* 25 (eds Sholle, P. & Schluger, P. R.) 17–43 (1979).
12. Nagy, B. & Mossman, D. J. *Early Organic Evolution: Implications for Mineral and Energy Resources* (ed. Schidlowski, M.) 224–231 (Springer, Heidelberg, in the press).
13. Lewan, M. D., Winters, J. C. & McDonald, J. H. *Science* **203,** 897–899 (1979).
14. Nagy, B., Leventhal, J. S. & Gauthier-Lafaye, F. *US Geol. Surv. Circ.* 1058, 65–67 (1991).
15. Leventhal, J. S. & Hofstra, A. H. *US Geol. Surv. Circ.* 1035, 42 (1988).
16. Choppin, G. R. *Radiochim. Acta* 44/45, 23–28 (1988).
17. Nagy, B., Thurman, E. M., Long, A. & Hare, P. E. *GSA Abstr. with Programs*, A173 (GSA, Boulder, 1988).
18. Loss, R. D. *et al. Chem. Geol.* **76,** 71–84 (1989).
19. Curtis, D. *et al. Appl. Geochem.* **4,** 49–62 (1989).
20. Loss, R. D. *et al. Earth planet. Sci. Lett.* **89,** 193–206 (1988).
21. Neuilly, M., Dozol, J. F. & Naudet, R. *Natural Fission Reactors*, 433–440 (IAEA, Vienna, 1978).
22. Ludwig, K. R., Nash, J. T. & Naeser, C. W. *Econ. Geol.* **76,** 89–110 (1981).
23. Holliger, P., Pagel, M. & Pironon, J. *Chem. Geol.* **80,** 45–53 (1989).
24. Bonhomme, M., Gauthier-Lafaye, F. & Weber, F. *Precambrian Res.* **18,** 87–102 (1982).
25. Holliger, P. *C. R. Acad. Sci. Paris* **307,** II, 367–373 (1988).
26. Ruffenach, J. C., Menes, J., Devillers, C., Lucas, M. & Hagemann, R. *Earth planet. Sci. Lett.* **30,** 94–104 (1976).
27. Ludwig, K. R., *Earth planet. Sci. Lett.* **46,** 212–220 (1980).
28. Loss, R. thesis, Univ. of Western Australia (1986).

ACKNOWLEDGEMENTS. We thank F. E. Lichte, S. MacFarland, J. McCrae and P. Mukhopadahay for technical assistance and N. H. Bostick, S. N. Davis, R. Hagemann, S. Moorbath, F.R.S., R. Naudet and F. Weber for commenting on the manuscript. This work was supported by the State of Nevada Nuclear Waste Project Office and Mifflin & Associates, Las Vegas NV, NATO Scientific Affairs Division and the Natural Sciences and Engineering Council of Canada.

© 1991 Nature Publishing Group